Chinese Chemical Letters 33 (2022) 5189–5195

Contents lists available at ScienceDirect

Chinese Chemical Letters

journal homepage: www.elsevier.com/locate/cclet

$CdBiO_2Br$ nanosheets *in situ* strong coupling to carbonized polymer dots and improved photocatalytic activity for organic pollutants degradation

Zhiyuan Pang[a], Bin Wang[a], Xingwang Yan[a], Chongtai Wang[b], Sheng Yin[a], Huaming Li[a], Jiexiang Xia[a,*]

[a] School of Chemistry and Chemical Engineering, Institute for Energy Research, Jiangsu University, Zhenjiang 212013, China
[b] School of Chemistry and Chemical Engineering, the Key Laboratory of Electrochemical Energy Storage and Energy Conversion of Hainan Province, Hainan Normal University, Haikou 571158, China

ARTICLE INFO

Article history:
Received 5 October 2021
Revised 30 November 2021
Accepted 20 January 2022
Available online 24 January 2022

Keywords:
Carbonized polymer dots
$CdBiO_2Br$
Direct Z-scheme heterojunction
Pollutant degradation
Photocatalytic activity

ABSTRACT

Carbonized polymer dots (CPDs) modified layer-structured $CdBiO_2Br$ (CPDs/$CdBiO_2Br$) Z-scheme heterojunction hybrid material has been synthesized *via* simple solvothermal method. The hybrid material with Z-scheme heterojunction can effectively maintain the original highly oxidizing holes of $CdBiO_2Br$ and the highly reducing electrons of CPDs. In addition, the construction of heterostructure is beneficial to the migration and separation of photogenerated carriers. Under visible light irradiation, 6 wt% CPDs/$CdBiO_2Br$ showed the best catalytic activity for degradation of organic pollutants. Free radical capture experiments and ESR analysis confirmed that the main active species are $^{\bullet}O_2^-$ and h^+. The decomposition process of organic pollutants was analyzed by LC-MS. Finally, the probable visible light mechanism performance of CPDs/$CdBiO_2Br$ as direct Z-scheme heterojunction photocatalytic materials was proposed.

Photocatalytic technology has gradually stood out among many catalytic methods [1,2], which can utilize inexhaustible and inexhaustible solar energy and is nontoxic to the environment [3,4]. However, the low efficiency of photogenerated carrier migration and separation can lead to the low activity of catalysts, which has become an urgent problem in photocatalytic technology [5,6]. Therefore, how to improve the carrier migration and separation efficiency is the current research focus in the field of semiconductor photocatalysis [7,8].

Layered-structured materials such as bismuth oxybromide (BiOBr) have attracted much attention in the most recent years for brand-new layered material structure in the field of environmental remediation and photocatalytic energy conversion [9,10]. BiOBr is characterized by nontoxicity, high stability, good photocatalytic activity and suitable band gap [11,12]. While suitable band gap determines its remarkable position in the photocatalysis field, while the covalent metal oxygen layers $[Bi_2O_2]^{2+}$ are separated by the halide layers along the (001) direction, forming an alternate structure with the double-layer halogen atoms [13,14]. However, the higher negative recombination rate of photogenerated electron-hole pair and the lower light absorption capacity still restrict the further development of BiOBr [15,16]. A part of Bi in the $[Bi_2O_2]^{2+}$ layer is replaced by other metal elements to form a covalent bimetallic oxide ion ($[ABiO_2]^+$, A = Ba, Sr, Ca, Pb, Cd, *etc.*) layer [17]. At this time, halide ion ($[X]^-$) layers are modified from double to single, $[ABiO_2]^+$ and $[X]^-$ are arranged alternately, the interlayer gap was greatly reduced, and carrier migration was easier due to the improvement of the passage, which could promote the generation of more reactive oxygen species [18]. On this basis, a hybrid cationic mix-layered catalyst, $CdBiO_2Br$, was developed to better promote the migration of photogenerated electron holes. However, after the electrons migrated to the surface of $CdBiO_2Br$, its separation process was not further improved [19,20].

Carbonized polymer dots (CPDs) have attracted much attention as a new type of carbon nanomaterial [21,22]. It has excellent characteristics of particle size less than 10 nm, spherical or quasi spherical morphology, and the surface has abundant polar groups (hydroxyl or carboxyl) [23,24]. Notably, CPDs have a unique conjugated π structure that can make it outstanding in electron transfer/storage properties and have also been successfully introduced into semiconductors, thus playing an improved role on photocatalytic performance. Combined with the above superiority of CPDs and $CdBiO_2Br$ ultrathin material, a novel Z-scheme com-

* Corresponding author.
E-mail address: xjx@ujs.edu.cn (J. Xia).

https://doi.org/10.1016/j.cclet.2022.01.054
1001-8417/

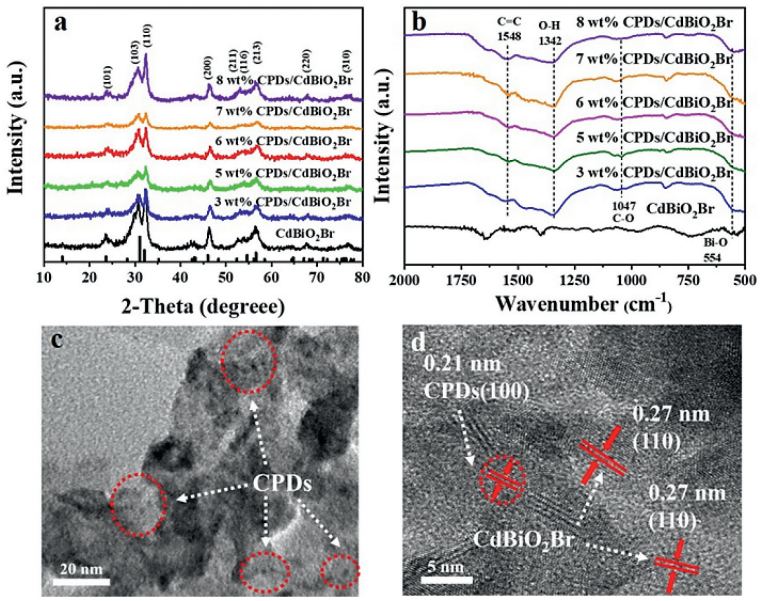

Fig. 1. (a) XRD pattern and (b) FT-IR of the as-prepared CPDs/$CdBiO_2Br$ samples with different contents of CPDs; (c) TEM and (d) HRTEM images of the 6 wt% CPDs/$CdBiO_2Br$ hybrid materials.

posite semiconductor photocatalytic system CPDs/$CdBiO_2Br$ was successfully constructed, which is greatly desired to gain simple and efficient photocatalytic materials to degrade organic pollutants [25,26].

In this paper, CPDs/$CdBiO_2Br$ hybrid materials were prepared by self-sacrificing ionic liquid glue at the first time. More CPDs could be anchored on the surface of $CdBiO_2Br$ materials *in situ* by the existence of Coulombic forces and hydrogen bonding interactions between ionic liquids and CPDs. The existence of intense physical and electronic coupling effects can make the migration and separation of photogenerated carriers at the heterojunction interface greatly improved. Construction of Z-scheme heterojunction, which can form a completely new carrier transport path, significantly inhibits the recombination of photogenerated electron holes and improves the separation efficiency of photogenerated carriers. This work points out a feasible direction for the design and preparation of simpler as well as more efficient photocatalytic materials for visible light degradation of pollutants.

The phase structures of the as-prepared CPDs/$CdBiO_2Br$ composite materials with different quantity of CPDs were analyzed by the characterization of XRD (Fig. 1a). All the diffraction peaks were of great consistence with the structure corresponding to the JCPDS No. 74–0239. Diffraction peaks located at 2θ values of 23.6°, 31.1°, 32.1°, 46.0°, 52.4°, 54.6°, 56.5°, 68.1° and 76.5° could be assigned to the (101), (103), (200), (211), (116), (213), (220), (310) and (317) crystallographic planes of the $CdBiO_2Br$, respectively. This result indicated the introduction of CPDs with present weight ratios does not have influence on the structure of $CdBiO_2Br$ material. Moreover, the signal about the CPDs could not be detected by XRD because the content of CPDs was low in the sample, which might be the good dispersion of CPDs in the CPDs/$CdBiO_2Br$ composite materials. Many previous literatures have reported these similar phenomena as well [27,28].

The possible interactions between CPDs and $CdBiO_2Br$ can get further confirmed *via* FT-IR analysis. The absorption bands at 554 cm^{-1} may be due to Bi−O stretching mode, which imply the existence of $CdBiO_2Br$ (Fig. 1b). The stretching vibrations of C=C at 1548 cm^{-1} and O−H at 1342 cm^{-1} can be observed for the CPDs/$CdBiO_2Br$ hybrid materials. Meanwhile, appearing peaks at 1047 cm^{-1} could be due to C−O, revealing the CPDs/$CdBiO_2Br$ hybrid materials possess the existence of CPDs [29]. Through the FT-IR spectra of the CPDs/$CdBiO_2Br$ hybrid, the characteristic peak at 555 cm^{-1} ascribed to Bi−O stretching mode tended to shift slightly higher, indicating the occurrence of interfacial interactions between CPDs and $CdBiO_2Br$.

To understand the flow direction of electrons and the chemical composition of these samples and the interaction between CPDs and $CdBiO_2Br$, XPS was performed [15,30]. Fig. S1a (Supporting information) showed the $CdBiO_2Br$ and CPDs/$CdBiO_2Br$ samples contained five elements of cadmium, bismuth, oxygen, bromine and carbon in the XPS survey scan spectra. The XPS high-resolution spectra Cd 3d for the $CdBiO_2Br$ and CPDs/$CdBiO_2Br$ samples are shown in Fig. S1b (Supporting information). The values of 411.9 eV and 405.1 eV in binding energies exist in the form of Cd^{2+} respectively. For the sample of $CdBiO_2Br$, the crystal structures of Bi $4f_{7/2}$ and Bi $4f_{5/2}$ of $[Bi_2O_2]^{2+}$ are corresponding to 159.0 eV and 164.6 eV, respectively. They are at the center of the spin orbit component of the Bi 4f peak as well (Fig. S1c in Supporting information). This suggests the existence of Bi^{3+} in the pure $CdBiO_2Br$ and CPDs/$CdBiO_2Br$. Compared to $CdBiO_2Br$ sample, the peak of Bi 4f in the CPDs/$CdBiO_2Br$ sample moves slightly to the higher binding energy, which indicates that the surface chemical environment of the element Bi in CPDs/$CdBiO_2Br$ hybrid has made some changes. The 531.3 eV and 529.9 eV value of oxygen in $[Bi_2O_2]^{2+}$ at O 1s peaks (Fig. S1d in Supporting information) result from the oxygen in the $CdBiO_2Br$ crystal. The slight shift of the O 1s peak in the CPDs/$CdBiO_2Br$ also indicates the change of chemical environment by the addition of CPDs. Similarly, it is known that the change of chemical environment also occurs on Br^-, as can be intuitively seen from the shift of Br 3d peaks (Fig. S1e in Supporting information) from 69.2 eV and 68.1 eV to 69.9 eV and 68.6 eV, which may be related to the presence of interaction between the $CdBiO_2Br$ and CPDs. Fig. S1f (Supporting information) displays the high-resolution XPS spectrum of C 1s, indicating that the main peak of 284.7 eV results from C−C bonds on sp^2 orbitals. The binding energies of 289.0 eV and 286.5 eV may be the center of the XPS peaks of C 1s, which are also resulted from C=O and C−O−C. XPS analysis results showed that the CPDs/$CdBiO_2Br$ hybrid has the existence of both $CdBiO_2Br$ and CPDs. The CPDs were modified and intimately integrated on $CdBiO_2Br$ successfully as a result.

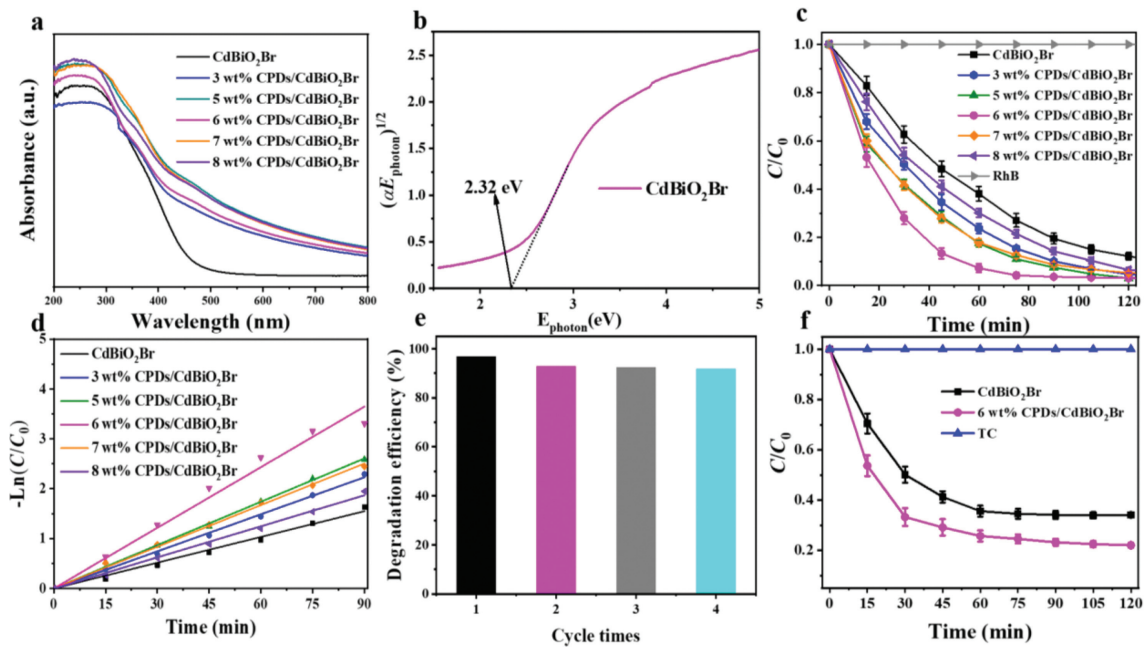

Fig. 2. (a) UV–vis diffuse reflectance spectra of the as-prepared CPDs/$CdBiO_2Br$ hybrid materials; (b) $(\alpha E_{photon})^{1/2}$ *vs.* E_{photon} curves; (c) photocatalytic degradation of RhB under visible light irradiation; (d) kinetic fit for the degradation of RhB; (e) cycling runs for the photodegradation of RhB; (f) photocatalytic degradation of TC in the presence of pure $CdBiO_2Br$, CPDs/$CdBiO_2Br$ hybrid materials under visible light irradiation.

To further investigate the microstructure of $CdBiO_2Br$ and CPDs/$CdBiO_2Br$ hybrid, TEM analysis was carried out. It could be seen that pure $CdBiO_2Br$ reveals porous ultrathin nanosheet structure (Fig. S2a in Supporting information), while the difference of crystal morphology is not great after the introduction of CPDs (Fig. S2b in Supporting information). From Fig. 1c, numerous dark dots are dispersed on nanosheets, which signifies CPDs have been introduced to $CdBiO_2Br$ uniformly. In the HRTEM image (Fig. 1d), the lattice fringe spacing of 0.27 nm and 0.21 nm belongs to the (110) crystallographic planes of $CdBiO_2Br$ crystallites and the (100) crystal plane of CPDs, respectively [31]. The crystallites of CPDs and $CdBiO_2Br$ have constituted an excellent combination, and the close mutual contact between the two crystal planes proved that the preparation of CPDs/$CdBiO_2Br$ hybrid material was successful.

The N_2 adsorption-desorption isotherms determination performed on the obtained hybrid samples can make the specific surface area determined (Fig. S3 in Supporting information). The values of specific surface were 93.90 m^2/g for pure $CdBiO_2Br$ and 122.47 m^2/g for 6 wt% CPDs/$CdBiO_2Br$, respectively. Obviously, with the introduction of CPDs into $CdBiO_2Br$, the value of specific surface area is raised obviously [32]. A higher BET specific surface area can get more and more active reactants and species absorbed at their surface, resulting in higher activity of photocatalysis after the improvement.

The optical and electronic properties of photocatalytic materials are also very important in terms of performance indicators. The optical absorption properties of CPDs/$CdBiO_2Br$ hybrid with different CPDs content and pure $CdBiO_2Br$ were analyzed through DRS, the results of which are displayed in Fig. 2a. The $CdBiO_2Br$ underwent an electronic transition from VB to CB under the irradiation of visible light and then displayed the onset of absorption at around 500 nm. Compared with pure $CdBiO_2Br$, the CPDs/$CdBiO_2Br$ hybrid exhibited an obvious red shift, and the light harvesting ability in the visible region was enhanced while the content of CPDs increasing. The band gap of $CdBiO_2Br$ is calculated to be around 2.32 eV (Fig. 2b) by the classical Tauc approach and the XPS valence band spectra for samples are corresponding to 2.13 eV (Fig. S4a in Supporting information). As shown in Fig. S4b (Supporting information), the flat band position of $CdBiO_2Br$ material was found to be −0.53 eV by Mott Schottky analysis, while positive slopes revealing $CdBiO_2Br$ to be an n-type semiconductor. Therefore, the VB of $CdBiO_2Br$ is 1.60 V *vs.* NHE. According to the formula $E_{CB} = E_{VB} - E_g$, the CB of $CdBiO_2Br$ is −0.72 V *vs.* NHE. Previous studies have revealed that the CB and VB of CPDs were −1.23 and −0.56 V *vs.* NHE, respectively, which reveal the energy bands of CPDs and $CdBiO_2Br$ are crossed [33,34].

Rhodamine B (RhB) is an additive of added pigments and the solution is purplish red, which is widely used in the staining of paper and leather. Despite being banned for food staining due to carcinogenesis, the abuse of RhB leads to its ubiquitous presence in surface water bodies and gradually raises environmental pollution problems, and a suitable degradation method is urgently needed to deal with RhB in water bodies. Therefore, the photocatalytic activities of the CPDs/$CdBiO_2Br$ and pure $CdBiO_2Br$ material were analyzed by degrading the coloured organic pollutant RhB. Fig. 2c displays the activities of pure $CdBiO_2Br$ and CPDs/$CdBiO_2Br$ hybrid with different amount of CPDs contents under the irradiation of visible light. Without catalyst, RhB almost did not undergo degradation and could be neglected, while different contents of CPDs may effectively improve the photocatalytic performance of $CdBiO_2Br$. Results showed that the 6 wt% CPDs/$CdBiO_2Br$ hybrid exhibited significantly higher activity than other CPDs containing hybrids and pure $CdBiO_2Br$ hybrids. Meanwhile, the kinetics of the photocatalytic degradation of RhB by CPDs/$CdBiO_2Br$ hybrids were investigated (Fig. 2d). The change concentration of RhB in CPDs/$CdBiO_2Br$ hybrid with irradiation time was fitted to the pseudo first order kinetic curve, while introducing CPDs could further improve the photocatalytic degradation rate [35]. Compared with pure $CdBiO_2Br$, the kinetic constant of 6 wt% CPDs/$CdBiO_2Br$ was raised from 0.017 min^{-1} to 0.041 min^{-1}, which was 2.41 times of pure $CdBiO_2Br$.

Any one simple and effective photocatalyst material, without good reusability and stability, its practical application would be greatly hindered. So, the recycling reaction for photodegradation of RhB on 6 wt% CPDs/$CdBiO_2Br$ hybrid was carried out by irradi-

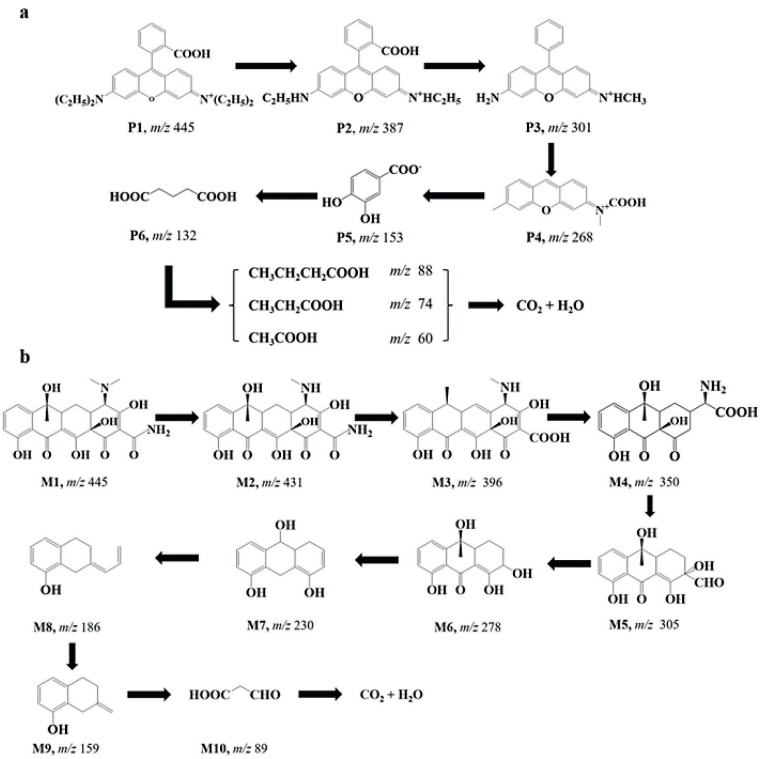

Fig. 3. Possible pathways of photocatalytic degradation of (a) RhB and (b) TC by 6 wt% CPDs/$CdBiO_2Br$.

ation of visible light to obtain the evaluation on the stability and reusability of CPDs/$CdBiO_2Br$ hybrid. After 4 consecutive cycles, the activity of the photocatalyst decreased by about 6%, implying that the CPDs/$CdBiO_2Br$ hybrid could maintain good stability and durability despite passing multiple cycles (Fig. 2e). Furthermore, XRD measurements and analysis of 6 wt% CPDs/$CdBiO_2Br$ before and after the photocatalytic reaction were performed. Fig. S5 (Supporting information). shows that the crystal structure has few changed, which reveal the CPDs/$CdBiO_2Br$ hybrid material is stable during the photodegradation process.

Tetracycline (TC) is a broad-spectrum antibiotic widely used for its remarkable bactericidal effect. However, the abuse of TC leads to the rising levels in water bodies and gradually evolves into an urgent environmental pollution problem. Therefore, the degradation and removal of TC are very important. Therefore, we performed visible light degradation of TC by photocatalytic materials while examining the photocatalytic activity of photocatalysts. The activity of the prepared CPDs/$CdBiO_2Br$ hybrid has been further appraised by catalytic degradation of antibiotic TC under visible light (Fig. 2f) [36]. It is shown that the 6 wt% CPDs/$CdBiO_2Br$ hybrid exhibited much higher than pure $CdBiO_2Br$ for TC photodegradation in photocatalytic activity. The degradation reached equilibrium after 60 min, at which point the photocatalytic degradation efficiency of CPDs/$CdBiO_2Br$ improved over 10% compared to pure $CdBiO_2Br$. The introduction of CPDs was effective to make the improvement of photocatalytic efficiency possible indicated by the results.

To further investigate the degradation courses of RhB and TC in photocatalysis, an in-depth analysis of possible intermediates was carried out using an LC-MS method. The characteristic MS signals of above intermediates are shown in Fig. S6 (Supporting information). For the degradation of RhB, Fig. 3a presents the possible course of RhB degradation by 6 wt% CPDs/$CdBiO_2Br$. The most initial RhB (**P1**, *m/z* 445) loses two ethyl groups first to produce intermediate material **P2** with a molecular weight of 387. In the subsequent degradation course, the above intermediate material again generates the intermediate product **P3** with a molecular weight of 301 by losing one carboxyl group, one methylene group, as well as one ethyl group. Immediately afterwards, **P3** undergoes carboxylation and generates **P4** by losing the phenyl ring and one methyl group (*m/z* 268). **P4** then undergoes oxidation, denitrification, and ring opening reactions to produce the dihydroxybenzoic or glutaric acid predominant carboxylic acids **P5** (*m/z* 153) and **P6** (*m/z* 132) and stepwise to smaller molecule carboxylic acids such as butyric, propionic, and acetic acids. Finally, by mineralization, CO_2 and water molecules are obtained [37].

Likewise, the characteristic MS signals of corresponding intermediates (Fig. S7 in Supporting information) as well as the potential pathway of TC degradation by 6 wt% CPDs/$CdBiO_2Br$ (Fig. 3b) were given. TC has a molecular weight of 445 (**M1**), and the product **M2** (*m/z* 431) could be generated by losing one *N*-methyl group. Upon the creation of a cavity, **M2** underwent further dealkylation dehydration to produce intermediate **M3** (*m/z* 396), which subsequently underwent sequential generation of **M4**, **M5**, and **M6** *via* carboxyl group removal, *N*-methyl group removal, and ring opening and oxidation reactions. Due to the action of h^+, subsequently, **M6** undergoes an elimination reaction and then generates **M7** (*m/z* 230) after removing the keto group and one methyl group. Continued through ring opening reaction to generate **M8**, **M9**, and further gave some small molecular species. In summary, under the action of active species, TC molecules undergo ring opening reactions and cleavage of functional groups (*N*-methyl, hydroxyl or amino) to finally degrade into carbon dioxide and water molecules to achieve efficient degradation under photocatalysis [38,39].

Electrochemical impedance spectroscopy (EIS) studies were put into effect on 6 wt% CPDs/$CdBiO_2Br$ and pure $CdBiO_2Br$ material samples for further investigation of the interfacial charge transfer resistance. The results exhibited that the arc radius on the EIS Nyquist curve of the 6 wt% CPDs/$CdBiO_2Br$ hybrid material sample

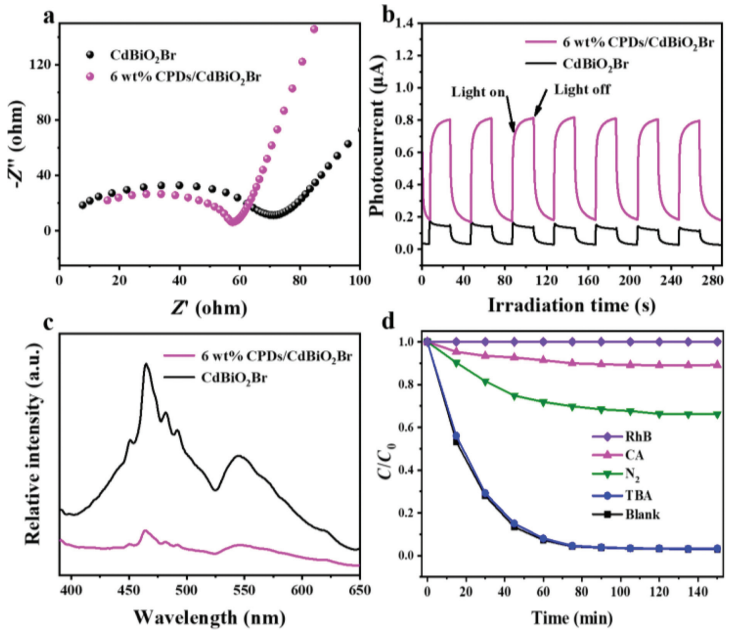

Fig. 4. (a) EIS; (b) transient photocurrent response and (c) PL spectra of the as-prepared CPDs/$CdBiO_2Br$ hybrid materials and pure $CdBiO_2Br$; (d) trapping experiment of active species during the photocatalytic degradation of RhB over CPDs/$CdBiO_2Br$ hybrid material under visible light irradiation.

was not as big as that of the pure $CdBiO_2Br$. The smaller the radius of the Nyquist circle is, the smaller the charge transfer resistance could become (Fig. 4a). The unique conjugated π structure of CPDs can be used as an effective transporter to accelerate the charge transfer at the interface and reduce the resistance [39]. This can allow the electron hole pairs to separate effectively, reaching the enhancement of photocatalytic efficiency finally.

Photocurrent curves of 6 wt% CPDs/$CdBiO_2Br$ and pure $CdBiO_2Br$ material electrodes are presented in Fig. 4b. When the illumination is activated, the response of photocurrent increases sharply, and it can maintain stable and reproducible performance within intermittent on-off irradiation for several cycles. CPDs is an excellent electron acceptor material with a unique conjugated structure, which can be an important condition for photoexcited carrier separation center. By taking advantage of the excellent conversion performance of CPDs, the electronic transitions of $CdBiO_2Br$ materials can be excited, which significantly promotes the efficient separation of photogenerated carriers of the composites. Compared to pure $CdBiO_2Br$, the CPDs/$CdBiO_2Br$ hybrid material exhibits a higher light absorption and photocurrent response the irradiation of visible light, while the photoexcited electron and hole separation rates are also relatively fast [40].

The charge migration, transfer and recombination processes of photocatalysts are the key links and can be studied by determining the photoluminescence (PL) spectra during chemical reactions [41]. The probability of recombination of photoexcited charge carriers decreases with decreasing intensity. The PL spectra of 6 wt% CPDs/$CdBiO_2Br$ and pure $CdBiO_2Br$ material are presented in Fig. 4c, indicating an emission peak of about 464 nm. The intensity of the emission band of CPDs/$CdBiO_2Br$ decreased significantly compared to that of $CdBiO_2Br$, implying that photoexcited electrons were effectively transferred from $CdBiO_2Br$ to CPDs when CPDs was anchored evenly onto the surface of CPDs/$CdBiO_2Br$. Consequently, introducing CPDs can effectively reduce the electron hole recombination rate of $CdBiO_2Br$, and thus effectively promote the charge separation of $CdBiO_2Br$ to achieve the purpose of improving the photocatalytic activity of $CdBiO_2Br$.

To further reveal the roles of the active species on the photocatalysis process over CPDs/$CdBiO_2Br$ materials, radical trapping experiments were performed with different scavengers (nitrogen (N_2) for $^{\bullet}O_2^-$, ammonium oxalate (AO) for holes, and *tert*–butanol alcohol (TBA) for $^{\bullet}OH$). As shown in Fig. 4d, when AO and N_2 were added, the degradation efficiency was greatly inhibited, indicating that holes and $^{\bullet}O_2^-$ were the main active components in the process of photocatalysis [42]. However, when TBA was added, the effect on photodegradation efficiency was hardly obvious, indicating no $^{\bullet}OH$ production [43].

The mechanism of CPDs/$CdBiO_2Br$ and the active species generated during photodegradation under visible light irradiation can be further validated by ESR analysis. This analysis employs 5,5-dimethyl-1-pyrroline *N*-oxide (DMPO) adsorbed on the photocatalyst or dissolved in methanol/water as a spin trap, allowing the detection of the spin reactivity $^{\bullet}OH$ and $^{\bullet}O_2^-$. The strong ESR spectra corresponding to DMPO-$^{\bullet}O_2^-$ adduct for both CPDs/$CdBiO_2Br$ and pure $CdBiO_2Br$ can be clearly observed (Fig. 5a) [44]. In addition, the ESR spectra intensity of DMPO-$^{\bullet}O_2^-$ adduct for CPDs/$CdBiO_2Br$ hybrid is significantly higher than pure $CdBiO_2Br$, indicating that more electrons are involved in the reaction of reducing O_2 to generate $^{\bullet}O_2^-$. The electron localized conjugation structure of CPDs makes the transfer of photogenerated electrons easier, thus achieving efficient separation of electron hole pair. While the DMPO-$^{\bullet}O_2^-$ was obvious, the DMPO–hydroxyl radical ($^{\bullet}OH$) species were not detected. This is due to the VB potential of both $OH^-/^{\bullet}OH$ (2.34 V *vs.* NHE) and $H_2O/^{\bullet}OH$ (1.99 V *vs.* NHE) are more positive than those of $CdBiO_2Br$ and CPDs, thus no $^{\bullet}OH$ production in terms of thermodynamics (Fig. 5b) [45].

We proposed the hypothesis that the as prepared CPDs/$CdBiO_2Br$ were conventional dual transfer structures, as shown in Fig. 5c. Then the electrons were excited from the CB of CPDs, transferred to the CB of $CdBiO_2Br$. However, the CB of $CdBiO_2Br$ is only 0.16 eV difference from the VB of CPDs, which would greatly increase the recombination rate of electrons on the CB of $CdBiO_2Br$ and holes on the VB of CPDs, greatly hindering the migration and separation of carriers. So, the holes in the VB of CPDs should combine with the electrons in the CB of $CdBiO_2Br$,

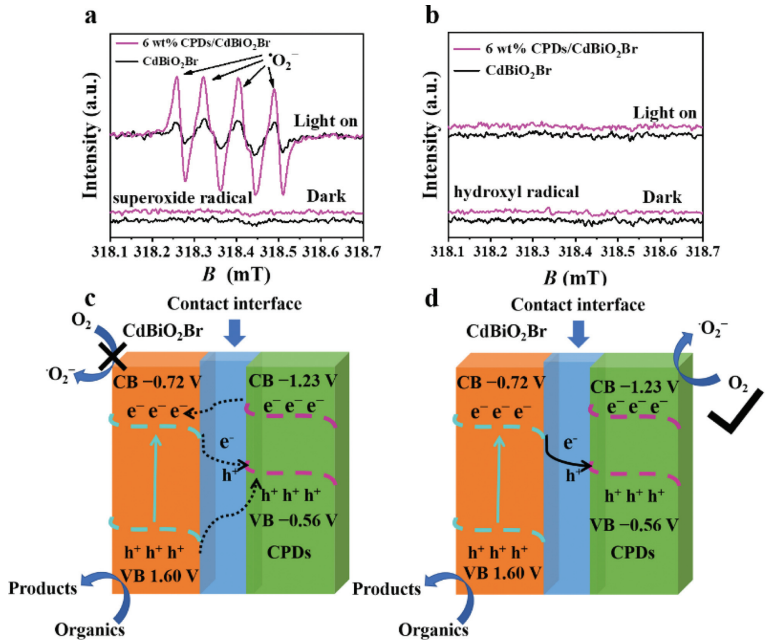

Fig. 5. (a, b) ESR spectra of radical adducts trapped by DMPO in CPDs/$CdBiO_2Br$ hybrid materials aqueous dispersion under visible light irradiation. Energy band diagram of (c) traditional photocatalytic system and (d) direct Z-scheme photocatalytic system for the CPDs/$CdBiO_2Br$ composite material.

which can effectively separate the electrons and holes and generate more active species, therefore, CPDs/$CdBiO_2Br$ is more likely to be a direct Z-scheme heterojunction structure (Fig. 5d).

In summary, a direct Z-scheme heterojunction photocatalytic material has been designed. A novel CPDs/$CdBiO_2Br$ photocatalytic material has been successfully constructed by introducing CPDs into the surface of $CdBiO_2Br$ *via* a simple solvothermal method, and the photocatalytic degradation activity of $CdBiO_2Br$ toward TC and RhB under the irradiation of visible light was improved by introducing CPDs for modification. Contrasting different mass fractions revealed that the 6 wt% CPDs/$CdBiO_2Br$ hybrid showed the best performance of photocatalysis. Moreover, the excellent stability and reusability of the CPDs/$CdBiO_2Br$ hybrid material play a vital role in the application of environmental protection. $^{\bullet}O_2^-$, and h^+ are the main active species in the process of photocatalysis. In summary, the efficiency of charge separation can be improved effectively by the introduction of CPDs and thus significantly improve the activity of photocatalysis at last. Various works in this thesis can also play important enlightening and guiding roles for the development and research of CPDs based photocatalytic hybrid material.

Declaration of competing interest

The authors declare that they have no known competing financial interests or personal relationships that could have appeared to influence the work reported in this paper.

Acknowledgments

This work was financially supported by the National Natural Science Foundation of China (No. 22108106, 21676128), China Postdoctoral Science Foundation (No. 2020M680065), Hong Kong Scholar Program (No. XJ2021021), Key Laboratory of Electrochemical Energy Storage and Energy Conversion of Hainan Province (No. KFKT2021005).

Supplementary materials

Supplementary material associated with this article can be found, in the online version, at doi:10.1016/j.cclet.2022.01.054.

References

[1] P. Li, Z. Zhou, Q. Wang, et al., J. Am. Chem. Soc. 142 (2020) 12430–12439.
[2] H. Zhang, Y. Wang, S. Zuo, et al., J. Am. Chem. Soc. 143 (2021) 2173–2177.
[3] T.T. Kong, Y.W. Jiang, Y. Xiong, J. Chem. Soc. Rev. 49 (2020) 6579–6591.
[4] Y.X. Yan, H. Yang, Z. Yi, et al., Environ. Eng. Sci. 37 (2020) 64–77.
[5] Y.Q. Wang, J.K. Wu, Y. Yan, et al., Chem. Eng. J. 43 (2021) 126313.
[6] R.A. He, R. Chen, J.H. Luo, S.Y. Zhang, D.F. Xu, Acta Phys. Chim. Sin. 37 (2021) 2011022.
[7] C.X. Zhao, Z.P. Chen, R. Shi, X.F. Yang, T.R. Zhang, Adv. Mater. 32 (2020) 1907296.
[8] Y. Lu, H. Zhang, D.Q. Fan, Z.P. Chen, X.F. Yang, J. Hazard. Mater. 423 (2022) 127128.
[9] E.H. Zhang, T. Wang, K. Yu, et al., J. Am. Chem. Soc. 141 (2019) 16569–16573.
[10] P.W. Zhou, L.P. Zhang, Y.M. Dai, et al., J. Cleaner Prod. 246 (2020) 119007.
[11] J. Sun, X. Li, Q. Zhao, B. Liu, Appl. Catal. B 281 (2021) 119478.
[12] X.J. Zou, C.Y. Yuan, Y.Y. Dong, et al., Chem. Eng. J. 379 (2020) 122380.
[13] Z.D. Wei, J.Y. Liu, W.J. Fang, et al., Catal. Sci. Technol. 8 (2018) 3774–3784.
[14] H.R. Zhou, Z.P. Wen, J. Liu, et al., Appl. Catal. B 242 (2019) 76–84.
[15] B. Wang, J. Di, L. Lu, et al., Appl. Catal. B 554 (2019) 551–559.
[16] Q.S. Wu, S.Q. Chai, H.P. Yang, et al., Sep. Purif. Technol. 253 (2020) 117388.
[17] J. Olchowka, H. Kabbour, M. Colmont, et al., Inorg. Chem. 55 (2016) 7582–7592.
[18] H.W. Huang, A.H. Reshak, S. Auluck, et al., J. Phys. Chem. C 122 (2018) 2661–2672.
[19] T.B. Ma, Y.S. Zhao, K.P. Ruan, et al., ACS Appl. Mater. Interfaces 12 (2020) 1677–1686.
[20] Z.W. Wang, M. Chen, D.L. Huang, et al., J. Chem. Eng. J. 374 (2019) 1025–1045.
[21] J.J. Liu, Y.J. Geng, D.W. Li, et al., Adv. Mater. 32 (2020) 1906641.
[22] B. Wang, J.Z. Zhao, H.I. Chen, et al., Appl. Catal. B 293 (2021) 120182.
[23] S.Y. Tao, S.Y. Lu, Y.J. Geng, et al., Angew. Chem. Int. Ed. 57 (2018) 2393–2398.
[24] Y.Y. Wang, H.L. Huang, Z.Z. Zhang, et al., Appl. Catal. B 282 (2021) 119570.
[25] M. Zhu, Z. Sun, M. Fujitsuka, T. Majima, Angew. Chem. Int. Ed. 57 (2018) 2160–2164.
[26] Q.L. Xu, L.Y. Zhang, B. Cheng, J.J. Fan, J.G. Yu, Chem 6 (2020) 1543–1559.
[27] J.Y. Liu, H. Xu, Y.G. Xu, et al., Appl. Catal. B 207 (2017) 429–437.
[28] H.W. Huang, Y. He, X. Du, P.K. Chu, Y.H. Zhang, ACS Sustain. Chem. Eng. 3 (2015) 3262–3273.
[29] R.L. Liu, D.Q. Wu, X.L. Feng, K. Mullen, J. Am. Chem. Soc. 133 (2011) 15221–15223.
[30] B. Wang, S.Z. Yang, H.L. Chen, et al., Appl. Catal. B 277 (2020) 119170.
[31] Y. Quan, B. Wang, G.P. Liu, H.M. Li, J.X. Xia, Chem. Eng. Sci. 232 (2021) 116338.
[32] Z. Tian, T. Chee, X. Zhang, L. Lei, C. Xiao, Chem. Eng. J. 412 (2021) 128687.
[33] L. Jiao, Y. Wang, H.L. Jiang, Q. Xu, Adv. Mater. 30 (2018) 1703663.
[34] X.X. Chang, T. Wang, J.L. Gong, Energy Environ. Sci. 9 (2016) 2177–2196.

[35] N. Belachew, D.R. Devi, K. Basavaiah, J. Mol. Liq. 224 (2016) 713–720.
[36] D.Q. Fan, Y. Lu, H. Zhang, et al., Appl. Catal. B 295 (2021) 120285.
[37] Z.J. Huang, Z. Lai, D.Y. Zhu, et al., J. Colloid Interface Sci. 597 (2021) 196–205.
[38] H.R. Sun, F. Guo, J.J. Pan, et al., Chem. Eng. J. 406 (2021) 126844.
[39] H.W. Huang, X. Han, X.W. Li, et al., ACS Appl. Mater. Inter. 7 (2015) 482–492.
[40] J.Y. Liu, H. Xu, J. Yan, et al., J. Mater. Chem. A 7 (2019) 18906–18914.
[41] F.Y. Liu, Y.M. Dai, F.H. Chen, C.C. Chen, J. Colloid Interface Sci. 562 (2020) 112–124.
[42] J. Chen, Z. Zhang, W. Zhu, et al., Environ. Res. 195 (2021) 110747.
[43] J. Chen, Z. He, Y. Jia, et al., Appl. Catal. B 257 (2019) 117912.
[44] Q. Yu, J. Chen, Y. Li, et al., Chin. J. Catal. 41 (2020) 1603–1612.
[45] P. Wei, D. Qin, J. Chen, et al., Environ. Sci. Nano 6 (2019) 959–969.